Dual-comb spectroscopy of molecular electronic transitions in condensed phases

Byungmoon Cho,[1] Tai Hyun Yoon,[1,2,*] and Minhaeng Cho[1,3,†]

[1]*Center for Molecular Spectroscopy and Dynamics, Institute for Basic Science (IBS), Seoul 02841, Republic of Korea*

[2]*Department of Physics, Korea University, Seoul 02841, Republic of Korea*

[3]*Department of Chemistry, Korea University, Seoul 02841, Republic of Korea*

(Received 25 January 2018; revised manuscript received 25 February 2018; published 16 March 2018)

Dual-comb spectroscopy (DCS) utilizes two phase-locked optical frequency combs to allow scanless acquisition of spectra using only a single point detector. Although recent DCS measurements demonstrate rapid acquisition of absolutely calibrated spectral lines with unprecedented precision and accuracy, complex phase-locking schemes and multiple coherent averaging present significant challenges for widespread adoption of DCS. Here, we demonstrate Global Positioning System (GPS) disciplined DCS of a molecular electronic transition in solution at around 800 nm, where the absorption spectrum is recovered by using a single time-domain interferogram. We anticipate that this simplified dual-comb technique with absolute time interval measurement and ultrabroad bandwidth will allow adoption of DCS to tackle molecular dynamics investigation through its implementation in time-resolved nonlinear spectroscopic studies and coherent multidimensional spectroscopy of coupled chromophore systems.

DOI: 10.1103/PhysRevA.97.033831

I. INTRODUCTION

The optical frequency comb has revolutionized the field of precision metrology [1,2] with the advent of mode-locked femtosecond lasers, octave spanning continuum generation from these lasers, and a direct link between optical frequency and the Cs atomic frequency standard [3,4]. The phase stabilization techniques [5,6] that enabled such achievements in metrology have found uses in spectroscopic applications of the optical frequency comb with remarkable successes [7–10].

In dual-comb spectroscopy (DCS), the mechanical time-delay scanning is removed by slightly off-setting one comb repetition rate with respect to another so that two sets of pulse trains have different but precise pulse-to-pulse time intervals. Taking each successive pair of pulses (one from each comb) at a time, this has the effect of increasing the time separation between the pairs after a complete overlap. The ability to phase-lock all frequency comb modes at once in the frequency domain allows unprecedented timing and frequency accuracy in *scanless* measurements with a fraction of acquisition time compared to conventional spectroscopy methods. The absence of moving parts, the capability to make phase coherent measurements, and use of a single point detector for broadband spectral measurements via fast Fourier transform bring significant advantages to many spectroscopic [11] and imaging [12] applications.

To successfully carry out DCS measurement, highly sophisticated phase-locking schemes, enhancement cavity, and/or multiple coherent averaging [13–15] were used. Notable works in the mid-IR frequency domain clearly demonstrated that DCS is an efficient tool for molecular fingerprinting [13] and trace gas detection [11]. Recently, the Cundiff group experimentally demonstrated a two-dimensional electronic spectroscopy of Rb vapor, developing heterodyne-detected dual-comb nonlinear spectroscopy [16]. Ideguchi *et al.*, using adaptive DCS, for the first time carried out DCS of the electronic transition of iodine in the gas phase [17]. However, molecules in condensed phases typically display much broader absorption lines than in the gas phase, which reflect the underlying dynamical processes, e.g., ultrafast dephasing of electronic coherence and short lifetimes of electronically excited states [18]. A frequency comb in the visible–near-infrared (vis-NIR) frequency domain that enables excitation of molecular electronic transition would bring the same powerful capability to spectroscopic investigation of molecular dynamics. In the present work, we report a broadband DCS of a dye solution whose absorption band is at around 375 THz. Here, both the repetition rate and the carrier-envelope-offset phase are locked to a Global Positioning System (GPS) disciplined atomic clock [19]. In Sec. II, we present detailed descriptions on our experimental setup and detection methods. The experimental and numerical simulation results with discussion are presented in Sec. III. The main results are summarized in Sec. IV with a few concluding remarks.

II. EXPERIMENTAL METHODS

A. Comb laser system

Here, we demonstrate DCS that uses a GPS-disciplined Rb clock (atomic clock) [20] to synchronize and phase-lock two comb lasers allowing the absolute measurement of the molecular spectrum of dye in solution (IR140 in ethanol) spanning 88 THz in the absorption bandwidth in the vis-NIR region with a single interferogram only. The schematic of our DCS setup is shown in Fig. 1. It consists of two comb lasers based on Ti:sapphire (Ti:Al_2O_3) oscillators having an optical

*thyoon@korea.ac.kr
†mcho@korea.ac.uk

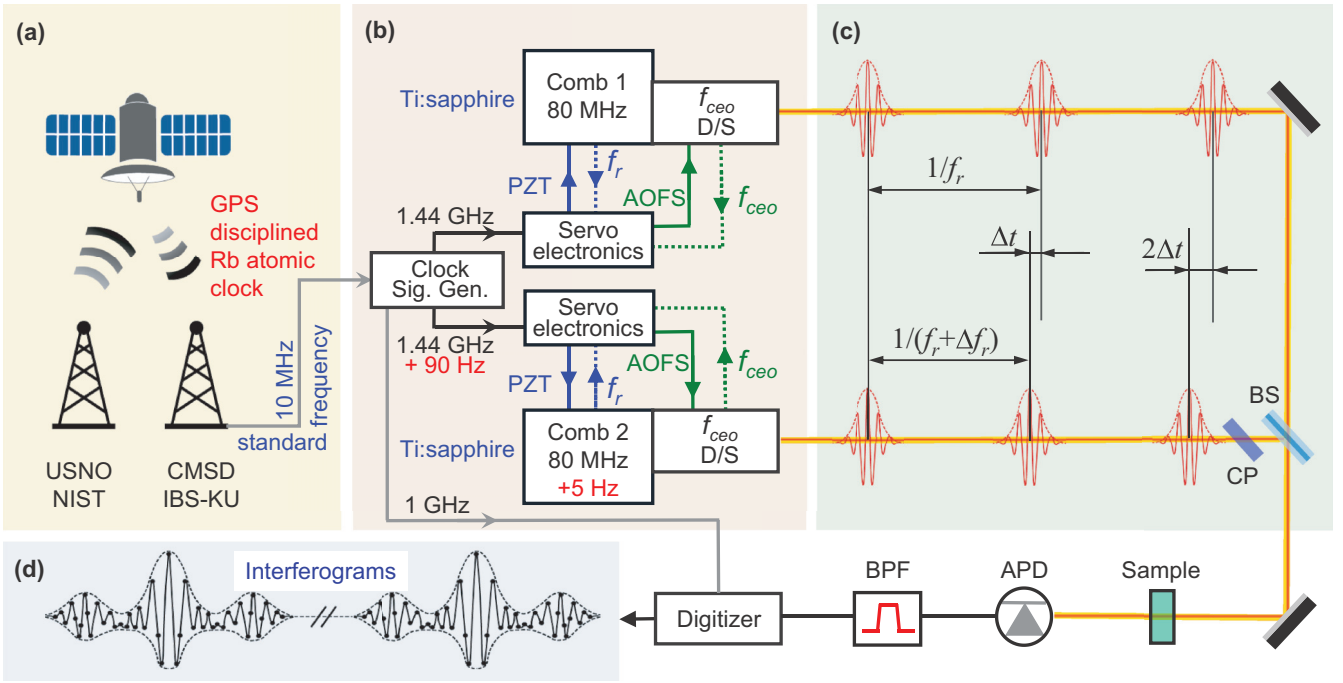

FIG. 1. Schematics of the absolute dual-comb spectroscopy setup based on mode-locked femtosecond Ti:sapphire ($Ti:Al_2O_3$) lasers. A mode-locked femtosecond laser emits a train of regularly time-spaced pulses and the time-averaged frequency output is described by a simple formula, $f_n = n f_r + f_{ceo}$, where f_n is the frequency of the nth comb mode, f_r is the laser repetition rate, and f_{ceo} is the carrier envelope offset frequency. In a frequency comb laser, f_r and f_{ceo} are measured and controlled: Here, the phase-locking loop maintains f_r with cavity length tuning and an external f_{ceo} detector-stabilizer (D-S) module detects f_{ceo} which is then mixed with f_r to be fed forward to the AOFS to set f_{ceo} to zero [20] (b). The servo electronics detect (dotted lines) and control (solid lines) radio frequencies f_r (blue) and f_{ceo} (green). For dual-comb spectroscopy, two comb lasers need to be synchronized. This is done by using a multichannel radio frequency clock signal generator that is phase locked to a 10 MHz rf standard from the GPS-disciplined Rb atomic clock (a). The phase-locked clock signals at the 18th harmonic of the repetition rates are delivered to the servo electronics to monitor and maintain f_r's of the two combs. The unit time delay is indicated by Δt which results from the difference in repetition rates (c). The interferograms are generated by sampling the "pulse pair event" at every $1/f_r$ which results in the generation of a single complete interferogram at every $1/\Delta f_r$. The fast digitizer phase locked with 1 GHz reference frequency from the clock signal generator samples the interferogram at 80 MHz (d). f_{ceo} D-S, f_{ceo} detector-stabilizer; BS, 50:50 beam splitter; CP, compensator plate; APD, avalanche photodiode; BPF, 15–35 MHz bandpass rf filter; AOFS, acousto-optic frequency shifter; PZT, piezoelectric transducer.

spectral bandwidth spanning over 120 THz around 800 nm. The laser system delivers ultrabroadband (~120 THz) pulses centered at ~800 nm (Fig. 2), where an intracavity dispersion management, including a pair of glass wedges and optics with broadband dielectric coatings mounted on ultraprecise motorized stages, was used; they need to be critically set by the user for the broadest bandwidth (Femtolasers, Rainbow^{TM} 2 CEP4). With the extracavity glass wedge and a pair of chirped mirrors, the chirp caused by pulse propagation through various dielectric media can be precompensated to generate near-transform-limited pulses at the sample position. The fringe-resolved intensity autocorrelations show that our system produces a few cycle pulses (~7 fs) at a 800-nm center wavelength (Fig. 3).

B. Phase-locking method

In the time domain, simultaneous monitoring and controlling of the phase of an optical electric field to enable phase coherent measurement would be tremendously challenging because concurrent detection and correction of phase (error) inevitably occur in series. In the frequency domain, on the other hand, phase coherence is guaranteed as long as the comb mode structure stays stable. This can be achieved by fixing the repetition rate (f_r) and carrier envelope offset frequency (f_{ceo}) to as precisely defined values as possible. Typically, f_r and f_{ceo} fall in the radio frequency (rf) range where the rf techniques enjoy tremendous precision and accuracy aided by phase-locking to a precise rf frequency standard, for example, a GPS-disciplined Rb atomic clock. This ability to transfer precision and accuracy of the rf standard to optical frequencies, thanks to a large value of comb mode number n, enabled the revolutionary progress in metrology. This approach enables novel ways to perform phase coherent spectroscopic measurements even in the optical domain.

We used a multichannel frequency synthesizer of which the time base is phase locked to the atomic clock for the phase locking of both repetition rate and carrier envelope offset frequency of each comb laser. In particular, a newly developed feed-forward method using an acousto-optic frequency shifter by Koke *et al.* was used to set f_{ceo} to zero for both combs [21]. The two comb lasers each possess an individual phase-locking servo loop to monitor and maintain repetition rate and carrier envelope offset frequency at precise values [Fig. 1(b)]. A distinct feature in our DCS is that the atomic clock [Fig. 1(a)] provides the frequency reference

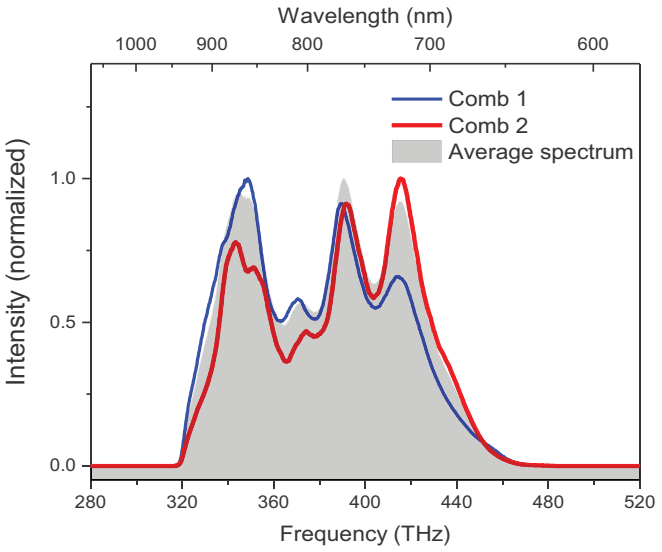

FIG. 2. Laser pulse spectra for comb 1 (thin blue line), comb 2 (thick red line) measured with a spectrometer with 1-nm resolution and the average of the two spectra (filled gray). The x axis is the frequency in THz, but the y axis is in arbitrary units. It should be noted that each spectrum is normalized by making the peak intensity to be unity. The spectrum (blue) of the comb 1 laser pulse peaks at around 350 THz, whereas that (red) of the comb 2 laser pulse peaks at around 420 THz. The average spectrum (gray) was measured by considering both pulse spectra peaks at around 400 THz. Here, these three spectra are compared to show their spectral shapes.

for the multichannel rf frequency synthesizer that delivers phase-locked rf signals at the 18th harmonic of 80 MHz, which corresponds to 1.440 GHz, to stabilize the repetition rate and carrier envelope offset frequency. The repetition rates of the two comb lasers can be independently set at sub-mHz level precision. Thus the repetition rate difference (Δf_r) set at the same level of precision means the corresponding time step size can be set with ~10 attoseconds (as) precision [Fig. 1(c)]. Because a single multichannel frequency synthesizer of which the time base is phase locked to the atomic clock can be used to synchronize the phases of f_r's and f_{ceo}'s of the two comb lasers, our DCS setup is believed to be simpler than those previously reported.

C. Dual-comb spectroscopy

The simple expression for comb mode frequency is $f_n = n f_r + f_{\mathrm{ceo}}$, where f_n is the frequency of the nth comb mode and n is the integer comb mode index. In dual-comb spectroscopy, the generation of an interferogram, in the form of a beat note between two combs essentially requires combs to obey $f_n = n f_r + f_{\mathrm{ceo}}$ for one and $f_m = m(f_r + \Delta f_r) + f'_{\mathrm{ceo}}$ for the other. Monitoring the repetition rates and offset frequencies of the two comb lasers and maintaining them at precisely fixed values are made possible through advanced and sophisticated rf electronics techniques [indicated as the servo electronics in Fig. 1(b)]. In our setup, the repetition rates are fixed by a phase-locking loop [6] controlling the cavity length by using a fast piezoelectric transducer and carrier envelope offsets by the acousto-optic frequency shifter based on feed-forward

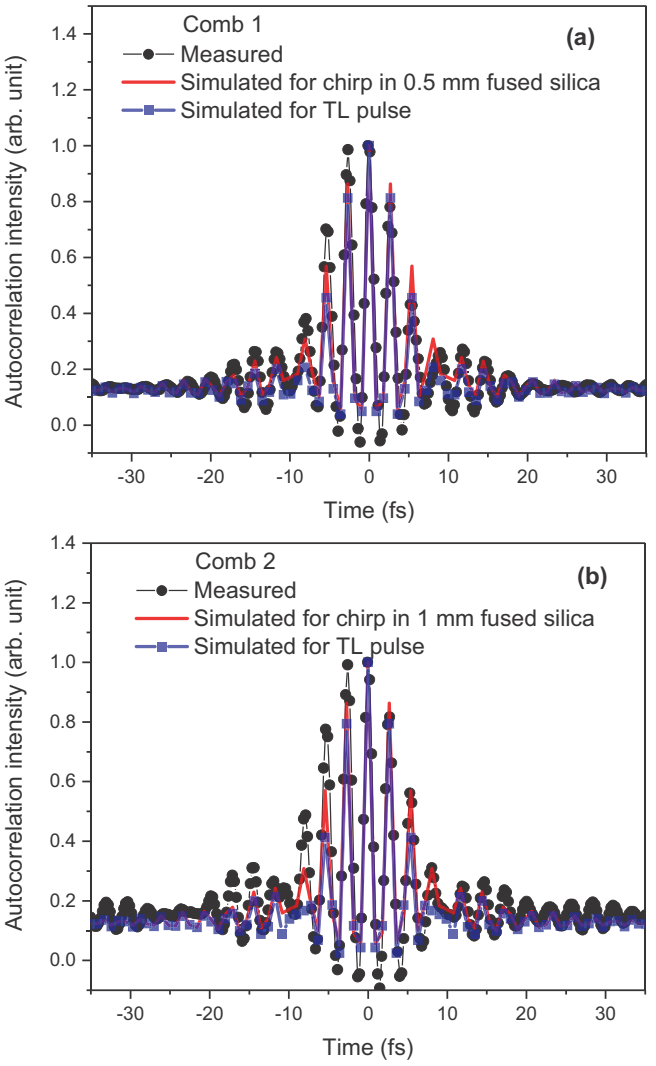

FIG. 3. Fringe-resolved intensity autocorrelation. The autocorrelations experimentally measured (black circle), numerically simulated for a chirped pulse (red), and numerically simulated for a transform-limited (TL) pulse (blue square) are shown for comb 1 (a) and comb 2 (b). For these numerical simulations, we considered group velocity dispersion (GVD), third-order dispersion (TOD), and fourth-order dispersion (FOD) in 0.5 mm (comb 1) and 1.0 mm (comb 2) thick fused silica with normally incident beams at 800-nm-center wavelength. Here, the measured comb spectra presented in Fig. 2 were used as inputs for numerical simulations with taking into account chirp effects.

extracavity correction to set f_{ceo} to zero [20]. The beam from the Ti:sapphire oscillator is split into two of which one beam is used for f_{ceo} detection and one for output (Fig. 4). The f_{ceo} detection employs a periodically poled lithium niobate crystal (PPLN) through which one beam passes and performs two functions simultaneously: (1) It broadens the spectra through nonlinear optical processes; (2) it facilitates the difference frequency generation (DFG) between low-frequency and high-frequency comb components in the broadened spectrum. The original and the DFG beams copropagate through the crystal and arrive at the avalanche photodiode (APD), creating a beat note between the original and DFG beams. This beat note

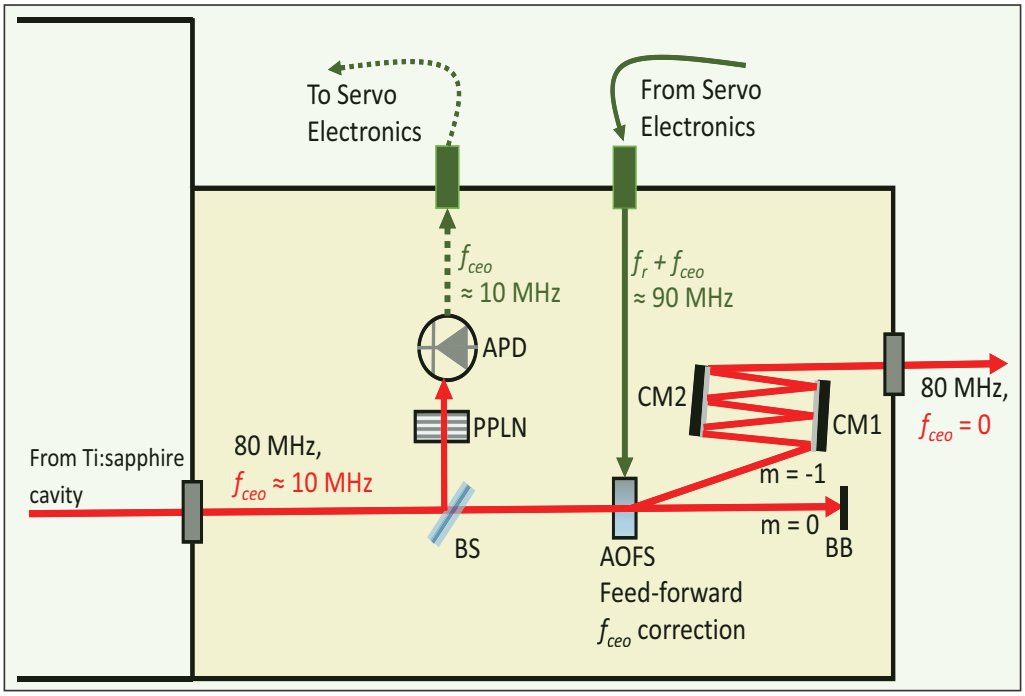

FIG. 4. Feed-forward method [21] for detecting and stabilizing f_{ceo}. The f_{ceo} frequency is detected in the beam that passes through the PPLN crystal as the beat note between the difference-frequency-generation (DFG) beam and the original beam at APD. This signal is fed into the servo electronic which mixes it with the repetition rate to drive AOFS. The $(m = -1)$st (the first negative diffraction order) diffraction component is picked off to be used as the main output from which measured f_{ceo} is subtracted to be zero. As mentioned in the main text, reference rf signals are generated by a multichannel rf synthesizer, which is synchronized to the 10 MHz standard frequency from a GPS-disciplined Rb atomic clock. A f_r stabilizer detects and phase-locks the repetition rate at $18 f_r = 1.440$ GHz by controlling the cavity length of the mode-locked laser, L. Fifty percent of the laser output is used to detect f_{ceo} with a DFG interferometer. The interference between DFG components and infrared components of the broadened frequency comb lines generates a beat note of $f_{ceo} \approx 10.0$ MHz. The other 50% of the laser output passes the AOFS driven by the f_{ceo} stabilizer with the frequency of $f_r + f_{ceo}$, so that the -1st-order diffracted beam has zero f_{ceo}. The chirp mirror pair (CM1 and CM2 in this figure) compensates the positive dispersion of the beam. BS, 50:50 beam splitter; PPLN, periodically poled lithium niobate crystal; APD, avalanche photodiode; AOFS, acousto-optic frequency shifter; CM1, CM2, chirped mirror; BB, beam block.

contains the f_{ceo} frequency and is sent to the servo electronics where it is mixed with f_r. The sum frequency of the detected f_{ceo} which varies from pulse to pulse and f_r which is fixed with a phase-locked loop is used to drive the acousto-optic frequency shifter (AOFS) through which the output beam passes. Here, we collect the $(m = -1)$st diffraction order with the result that the detected f_{ceo} is subtracted from the output beam (shifting the whole comb by f_r is equivalent to a 2π phase shift and leaves the comb unchanged). This is the so-called feed-forward method because the detected f_{ceo} is used to correct for the other half of the beam used for the output [21].

D. Synchronization of two comb lasers

To perform dual-comb spectroscopy, not only does one need to ensure phase coherence in the pulse train but also the two comb lasers must be synchronized so that there is phase coherence between the two separate pulse trains. The latter condition typically requires complex schemes; this has been pointed out as one of the major reasons hindering wider adoption of dual-comb spectroscopy. Such schemes are significantly challenging, as briefly mentioned in the Introduction. For example, to generate high-quality interferograms and thus broad spectra, coherent averaging of many tens to hundreds of thousands of interferograms were required [14], adaptive sampling to correct the time base was used [15], samples had to be placed in a cavity to increase absorption [13], and complicated frequency locking of a few comb modes to stabilized cw lines was used [14]. In our case, a relatively straightforward synchronization of the two combs is achieved by supplying phase-locked rf frequency signals for repetition rates from a single multichannel rf frequency synthesizer (Holzworth, HS9008A). Another unique feature of the present DCS setup is that we use the GPS-disciplined Rb atomic clock signal as the absolute reference for the multichannel rf synthesizer, which makes the synchronization of the two comb lasers very easy and simple.

E. Dual-comb interferogram

It is well known that there is a close analogy between the dual-comb interferogram and that of the time-delay scanning Fourier transform infrared (FTIR) spectroscopy. In an FTIR based on a Michelson interferometer, a light beam from a single source is split into two by a beam splitter where one of the beams experiences retardation via a mechanically variable optical path, causing constructive and destructive interference as a function of retardation resulting in the interferogram. In DCS, the single light source is replace by the comb lasers and both comb beams combine at the beam splitter; a sample

may be placed before (only one comb passes the sample) or after the beam splitter (both combs pass the sample). A low-noise high-bandwidth photodetector placed after the beam splitter measures the signal as a function of time. Because the pulse-to-pulse time intervals are $1/f_r$ and $1/(f_r + \Delta f_r)$ for the first and second comb, respectively, the time delay (the difference in time interval between combs) is $\Delta t = \Delta f_r / f_r^2$ for $f_r \gg \Delta f_r$. Thus, after a time coincidence of the pulse pair, every successive pair has a linearly increasing time gap equaling the multiples of Δt and the analogous interferogram signal is generated in a *scanless* manner.

F. Sample signal detection method

A fused silica cuvette containing the sample was placed between the beam splitter that combines the two beams from the comb lasers and the avalanche photodiode (APD, Menlo Systems, APD210). In a 2-mm-thick sample, peak absorbance was 0.4 (13 μM concentration). A rotating magnetic microstirrer bar inside the cuvette circulated the sample. The two beams from the comb lasers were unfocused, had a diameter around 3 mm at the sample, and had power ~1 mW before the sample (~20% excitation probability). After passing once through the sample, the beams reached the APD with the same diameter (the area of the sensor is 0.5×0.5 mm^2 so the beam overfills the sensor). A variable neutral density filter in front of the APD adjusted the power for an optimal interferogram signal. The oscillating voltage signal from the APD first passes through rf bandpass filter and is sampled at 80 MHz with a high-speed digitizer (Spectrum, M3i.4861-EXP) which is synchronized to an atomic clock.

G. Numerical simulation methods

In the present work, we also carried out numerical simulations of time-domain interferograms, taking into account the effect of chirp (up to third order), nonzero carrier envelope offset frequency, and absorptive and refractive effects of the sample, to see how they manifest themselves in the vis-NIR broadband interferograms. Interferogram simulations were carried out for through-air, ethanol blank, and IR140 sample cases which were then compared to those measured to discern if the observed differences indeed have a basis in the above-mentioned factors. Equation (1) describes the time-dependent electric field pulse train, $E(t)$, that has undergone attenuation and refraction as well as chirp:

$$E(t) = \mathrm{Re}\left(\sum_i a_i \exp[i\omega_i t - \kappa_A(\omega_i) + i\phi_A(\omega_i) + i\phi_{\mathrm{chirp}}(\omega_i)]\right), \tag{1}$$

where a_i is the amplitude of the comb mode i, which is determined by the measured comb spectrum, ω_i is the angular frequency of the comb mode i, $\kappa_A(\omega_i)$ is the attenuation factor due to the absorbance of the comb mode at frequency ω_i, $\phi_A(\omega_i)$ accounts for the phase shift due to free induction decay induced in the sample by the incoming field, and $\phi_{\mathrm{chirp}}(\omega_i)$ represents the frequency-dependent chirp effect on the electric field phase. Note that the first comb mode has zero frequency when the carrier envelope offset is zero.

Two sets of electric pulse trains are simulated from comb spectra via Fourier synthesis according to Eq. (1). Here, discrete frequency oscillations with equal frequency interval are summed in the time domain grid. The summation generates an electric field pulse train for comb 1, $E_1(t)$, and comb 2, $E_2(t)$. The repetition rate offset between the two sets of electric pulse trains given by Δf_r determines the interval in the time grid (i.e., the time step size for the simulation).

As the two time-dependent electric pulse trains impinge on the photo detector, the time-dependent heterodyne signal is generated according to Eq. (2).

$$I(t) = |E_1(t) + E_2(t)|^2. \tag{2}$$

The measured interferogram signal on a slow square-law photodetector is simulated as follows [Eq. (3)]: The two pulse electric field trains are summed [Eq. (2)] and pairwise integrated at the repetition rate interval over the detector response time.

$$I_{\mathrm{interferogram}}(\tau) = \int_{-\infty}^{\infty} R_{\mathrm{det}}(\tau - t) I(t) dt, \tag{3}$$

where $R_{\mathrm{det}}(t)$ is the detector response which is typically on the order of a nanosecond.

In the simulations, the repetition rate, $f_r = 2500$ GHz, and the difference in the repetition rate, $\Delta f_r = 3$ GHz, were used, just for the sake of computational simplicity. Note that if the same experimental f_r and Δf_r values for simulations (80 MHz and 5 Hz, respectively) are used, the spectra have too high a comb density (~1.9×10^6 comb modes), making the pulse interval too large (12.5 ns), which makes numerical computations a bit difficult. With these parameters, the conversion factor is 833.33^{-1} (=1.2×10^{-3}) so 800 nm (375 THz) optical oscillation is downconverted to 450 GHz. There were 222 comb teeth starting from the zero frequency and, over the comb spectra for which measured spectra were used as input, there were 121 comb teeth. For Fourier synthesis, the Fourier components were summed on the time grid with 2^{22} (=419 430 4) grid points, resulting in 2.011 ns total time span. Full interferograms are generated every 333.3 ps. The chirp was calculated to the third order in fused silica (FS) using the Sellmeier equation for 0.5 mm (for comb 1) and 1 mm (for comb 2) thickness and 800-nm-center wavelength. For 0.5-mm-thick FS, group velocity dispersion (GVD) = 18.081 fs^2, third-order dispersion (TOD) = 13.749 fs^3, and fourth-order dispersion (FOD) = −5.717 fs^4; for 1.0-mm-thick FS, GVD = 36.162 fs^2, TOD = 27.497 fs^3, and FOD = −11.435 fs^4. The simulated transmittance and absorbance spectra of IR140 in ethanol match those measured with a spectrometer and were recovered from the interferograms within ~10% error.

III. RESULTS AND DISCUSSION

A. Interferograms in time domain

Figure 5(a) displays the raw 3.4-s scan trace showing 17 interferograms for IR140, which is a dye molecule, dissolved in ethanol and measured in a symmetric configuration (both beams experience the sample [11]). In Fig. 5(b), one of

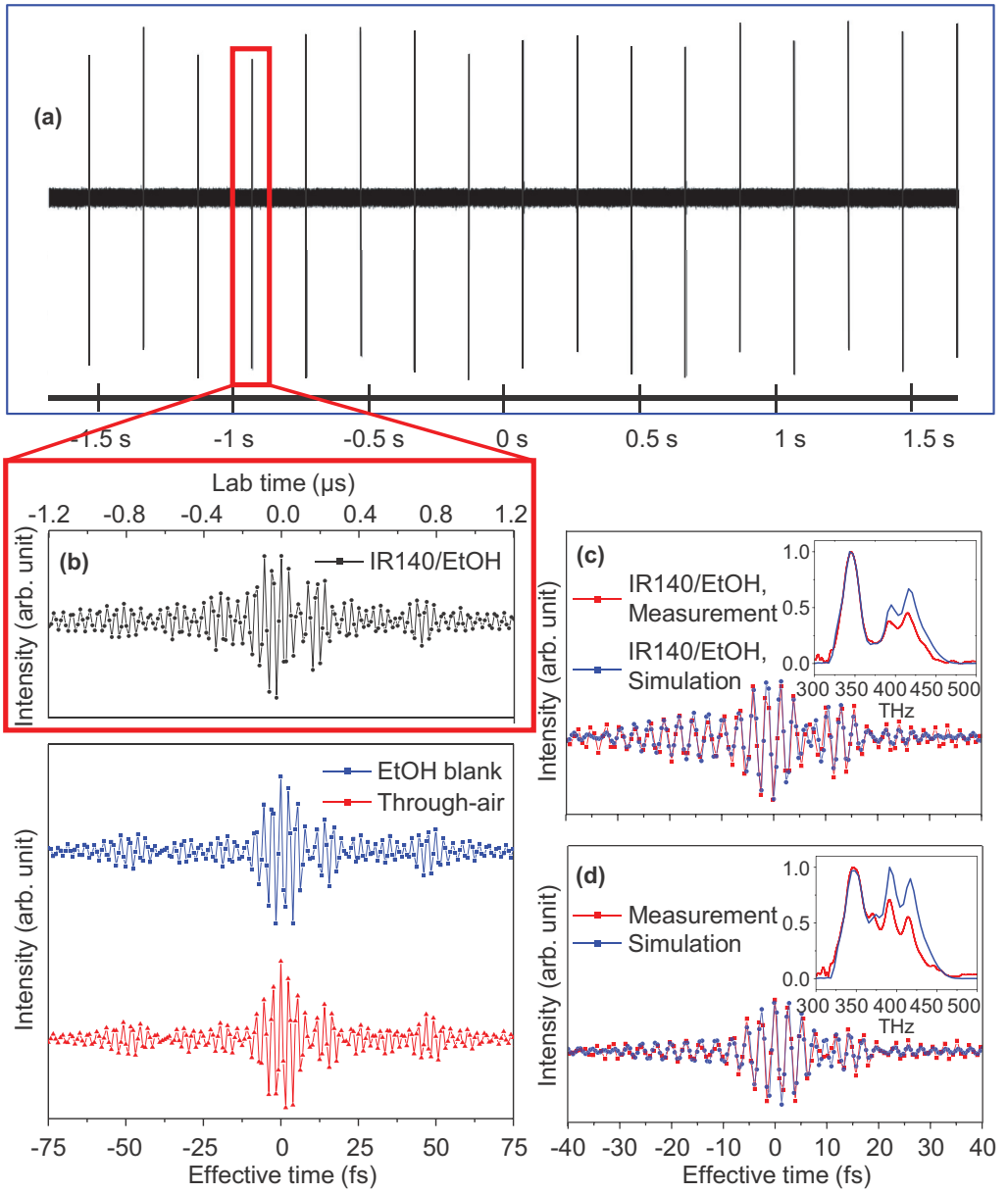

FIG. 5. Dual-comb raw interferograms (a,b), numerically simulated interferograms (c,d), spectra recovered from the interferograms via Fourier transformation (e), and transmittance and absorbance spectra of IR140 in ethanol (f). (a) A set of 17 IR140 in ethanol interferograms measured in a single scan taking ∼3.4 s in lab time, ∼210 ns in effective time). Interferograms are generated every 0.2 s $[1/\Delta f_r]$. (b) One of the raw interferograms of IR140 in ethanol (upper panel, black circle), ethanol blank (lower panel, blue square), and air (lower panel, red triangle) are zoomed in. A single interferogram spans ∼3 μs (∼240 data points) before the signal reaches the level indistinguishable from the noise. Each point is sampled every 12.5 ns $[1/f_r]$. Traces are offset for clarity in (b). (c,d) Simulated interferograms (blue circle) compared with measured interferograms (red square) and the respective spectra (insets: simulations in blue and measurements in red) for IR140 in ethanol sample (c) and ethanol blank (d).

the IR140 interferograms is zoomed in (top panel) and for comparison, identically measured ethanol blank and through-air interferograms are shown (bottom panel). In our DCS measurements, the repetition rates were 80 MHz for comb 1 and 80 MHz + 5 Hz ($\Delta f_r = 5$ Hz) for comb 2. The unit time delay, due to this Δf_r, was therefore 781.25 as because it is determined by the repetition rates and their differences of the two comb lasers, i.e., $\Delta t = \Delta f_r / f_r^2$. The pulse pairs with the increasing time delay between them impinge the sample at every 12.5 ns [1/(80 MHz)]. At the slow square-law detector with 500-ps rising time, the sum of the two electric fields is integrated, generating an oscillating voltage signal with the successive arrival of pulse pairs.

Imprinted in this time-varying intensity is the information about the electric fields that generated it; the fields that interacted with a sample will, in turn, contain information about the sample. In the frequency domain picture, the slight difference in the repetition rate is equivalent to a slight difference in the frequency comb spacing between two combs. Each comb pair, therefore, differs in integer multiples of a frequency difference

set by the repetition rate difference Δf_r, and the avalanche photodiode (APD), at which the summed fields is integrated, detects the beat signal between the two electric fields with slightly different optical frequencies. In our setup, this beat signal appears in the rf range; the degree of this downconversion from an optical frequency to rf is determined by the ratio of the difference in the repetition rate and the repetition rate itself, i.e., $\Delta f_r/f_r = (16\times10^6)^{-1}$. For example, a 375 THz optical oscillation (~800 nm) will be downconverted to 23.4 MHz rf oscillation where the rf bandpass filter can select the beat notes with reduced high- and low-frequency noises. This scaling factor is important in allowing mapping of optical frequency into rf and enables detection using rf electronic devices. The fast optical oscillation can be followed directly through heterodyning; in a sense, the speed of the oscillation is stretched in time by this factor so a femtosecond oscillation period in effective time may manifest as nanoseconds oscillation in lab time. This downconversion works in much the same way as it does in a conventional FTIR spectrometer where the ratio of the velocity at which the mirror in the interferometer is scanned and the speed of light determines the downconversion factor [22] and so the observed frequency appears to be much slower; the true frequency is easily recovered by multiplying back by the inverse downconversion factor. The broad electronic absorption spectrum reflecting ultrafast relaxation dynamics such as electronic dephasing [18] [e.g., $1/T_2 \approx (10\,\text{fs})^{-1} = 100\,\text{THz}$] means that it is only possible to fully sample this optical frequency signal (i.e., satisfying Nyquist sampling criterion) with rf electronics with 10^6-10^7 downconversion.

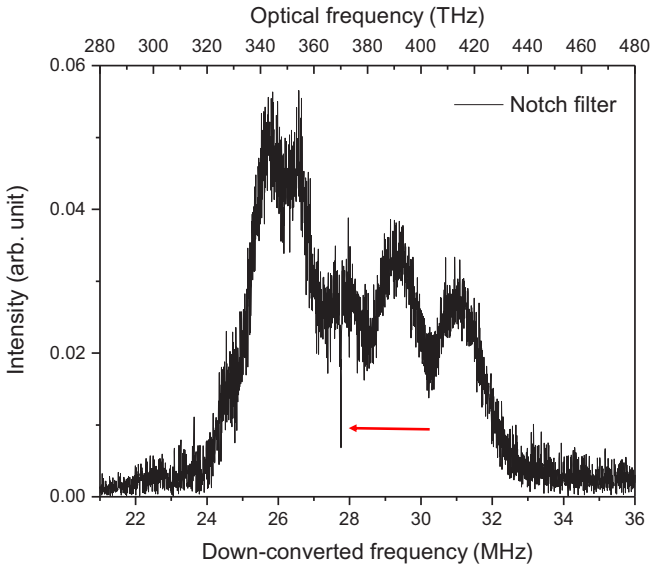

FIG. 6. Single-interferogram DCS measurement of a notch filter showing the notch-bandwidth-limited dip at ~371 THz optical frequency, ~27.8 MHz downconverted frequency. The manufacturer (Ondax) specifications were $<10\,\text{cm}^{-1}$ (0.15 nm) at ~808-nm-center wavelength. The measured width of the dip is $\sim\pm2.5\,\text{cm}^{-1}$ (75 GHz). The measured interferogram spanned -136.7 to $+132.356\,\mu\text{s}$ in lab time (-10.2523 ps to $+9.9267$ ps in effective time). The total lab time range was $269.061\,\mu\text{s}$ (total number of sampled points in the interferogram: 48 431). $\Delta f_r = 6$ Hz (downconversion factor 7.5×10^{-8}). No zero padding was applied.

B. Frequency range and resolution

The major advantage of the DCS is that optical oscillation phase coherence is maintained throughout the course of the measurements, which has been challenging with conventional mechanical time-delay scanning for optical frequency oscillation or even with an adaptive sampling scheme in previous DCS [15]. The single scan trace containing 17 interferograms [Fig. 5(a)] was recorded with a fast digitizer at an 80 MHz sampling rate synchronized to the atomic clock signal so an interferogram is generated at every 0.2 s ($=1/\Delta f_r = 1/5\,\text{Hz}^{-1}$). Illustrating the scan efficiency in dual-comb spectroscopy, the 0.2-s full single-interferogram recurrence time in the lab time is equivalent to the 12.5-ns total scan time in the effective time; with a conventional mechanical delay stage in a double pass arrangement, the length of the stage needed would be 1.874 m. To obtain an equivalent full single interferogram, 16×10^6 data points would need to be sampled at the 781.25-as time step (117 nm in a double pass arrangement), and to average, repeated multiple times. Generation of high-quality interferograms that enable extraction of molecular information thus requires a remarkable degree of phase coherence, in particular, for vis-NIR pulses (an 800-nm single cycle oscillation is 2.67 fs). Here, the two sets of few-cycle optical laser pulse trains that each has the bandwidth ~120 THz (so contains $\sim1.9\,10^6$ comb modes at 80 MHz comb spacing) must maintain phase coherence between all comb modes and over the measurement time as demonstrated in this paper.

The optimum value of Δf_r can be chosen by considering the balance between a speedy acquisition (as big a step size as possible) and remaining within the Nyquist sampling criterion (limit on the step size). The downconverted bandwidth must be less than one half of the optical sampling free spectral range (i.e., $f_r/2$) to map all optical frequencies into rf [11]: $\Delta\nu_{\text{optical}}\,\Delta f_r/f_r \leqslant f_r/2$, where $\Delta\nu_{\text{optical}}$ ($\approx$120 THz) is the optical bandwidth. Because of the large downconversion factor (16×10^6), despite the ultrabroad optical bandwidth, the whole optical spectrum compresses into <10 MHz. In fact, the largest Δf_r allowed is 21.3 Hz in this limit and the corresponding step size of 3.33 fs already exceeds one half of the period of optical oscillation. To avoid aliasing due to undersampling, the upper bound of Δf_r is determined by the time domain Nyquist sampling criterion that is ~8.55 Hz (1.33-fs step size).

The choice of Δf_r also sets the frequency range and resolution that are given by inverse time step size, $(\Delta f_r/f_r^2)^{-1}$, and inverse total time scan, $[N(\Delta f_r/f_r^2)]^{-1}$, respectively ($N$ is the total number of sampled data points that equals $f_r/\Delta f_r$ so total scan time is $1/f_r$). In our case, the maximum frequency resolution at the comb spacing of $f_r = 80$ MHz equals ~2 parts per million (Fig. 6) and the minimum spectral range using the largest time step size of 1.33 fs ($\Delta f_r = 8.55$ Hz) equals 752 THz, ~10 times the width of the absorption band. Both conditions exceed the requirement to capture the whole absorption spectrum and spectral features.

C. Numerical simulations of time-domain interferograms

For few-cycle pulses covering ~170-nm bandwidth around 800 nm, sample absorption and chirp likely have noticeable effects. Since no molecular interferograms generated by

interaction of such short pulses with a broad electronic transition have been reported, pulse propagation effects were to be investigated by numerical simulations. In simulating a downconverted optical signal in the form of an interferogram, we used the measured IR140 in ethanol absorption spectrum as well as the measured comb laser spectra as inputs. From this, with the Kramers-Kronig relation, the sample free induction decay and complex susceptibility were obtained [23]. In addition, the material chirp was accounted for up to third order in fused silica (see Sec. II G). The simulation can account for a slight variation of f_{ceo} from zero, which has an effect of shifting the entire set of one-comb modes with respect to the other (only the difference, Δf_{ceo}, matters): this was input as a fraction of the comb spacing. In the simulations, this ranged from 0.2% to 0.5% of the comb spacing.

The simulations [Figs. 5(c) and 5(d)] reveal that in the symmetric configuration (both combs interact with the sample and reference), the interferograms are always symmetric around the center burst (zero time delay). The apparent asymmetry in the measured interferograms in Fig. 5(b) are caused mainly by the differential chirp. Here, comb 2 experiences more chirp than comb 1 equivalent to ∼0.5 mm extra thickness of fused silica. Note that when both combs have the same chirp, the resulting interferogram should be symmetric and identical to that without any chirp. The differences in IR140 in ethanol and ethanol blank interferograms are well reproduced. Such differences in features are faithfully generated only when sample free induction decay effects are accounted for in addition to the chirp in IR140 in ethanol. Note that the field attenuation only (i.e., using only the imaginary component of the complex refractive index function) could not fully reproduce the experimental results.

D. Carrier-envelope-offset frequency locking

The interferograms shown in Fig. 5(a) were obtained by maintaining repetition rates of the two comb lasers constant and controlling the absolute f_{ceo} values of the two lasers to be zero. Although one can obtain good signal-to-noise (SNR) interferograms by sacrificing frequency resolution, it is believed that coherence between the two lasers is a prerequisite for the generation of high-SNR interferograms and is crucial for the single-interferogram extraction of molecular spectrum. Without the phase stability of millions of comb modes and between two sets of such comb modes, absolute even time spacing could not be achieved and the interferogram would simply wash out. As shown in Fig. 5(a), there is an over-3-s time trace containing 17 interferograms indicating remarkable electric field oscillation phase coherence with few cycle pulse trains of ∼6 fs for a significant time duration. Of course, a narrow time window for sampling data could improve the SNR, but this is not the main reason for a good SNR in our spectrum. To illustrate this, we considered an expanded time window by a factor of 12 (60-μs interferogram instead of 5-μs interferogram), compared the resulting Fourier-transformed spectrum with that obtained with a narrow (5-μs) time window, and found that the SNR is not degraded by the same factor of 12.

To further emphasize the importance of phase coherence to obtain good SNR interferograms and resulting Fourier-transformed spectra, we include Fig. 7 which shows two different interferograms [Fig. 7(a)] and their Fourier-transformed spectra [Fig. 7(b)]. When one of the f_{ceo} locking servos [see Fig. 1(b)] is turned off [Fig. 7(a), red], the noise amplitudes in the interferogram increases by at least a factor of 10 compared to the one with both f_{ceo} locking servos on, which corresponds to our experimental condition described above. Furthermore, the absorption spectra [Fig. 7(b), red] cannot be retrieved from the interferogram obtained without f_{ceo} lockings of both comb lasers. This strongly supports the notion that the phase synchronization (coherence) is prerequisite for achieving good SNR measurements of interferograms and resulting spectra.

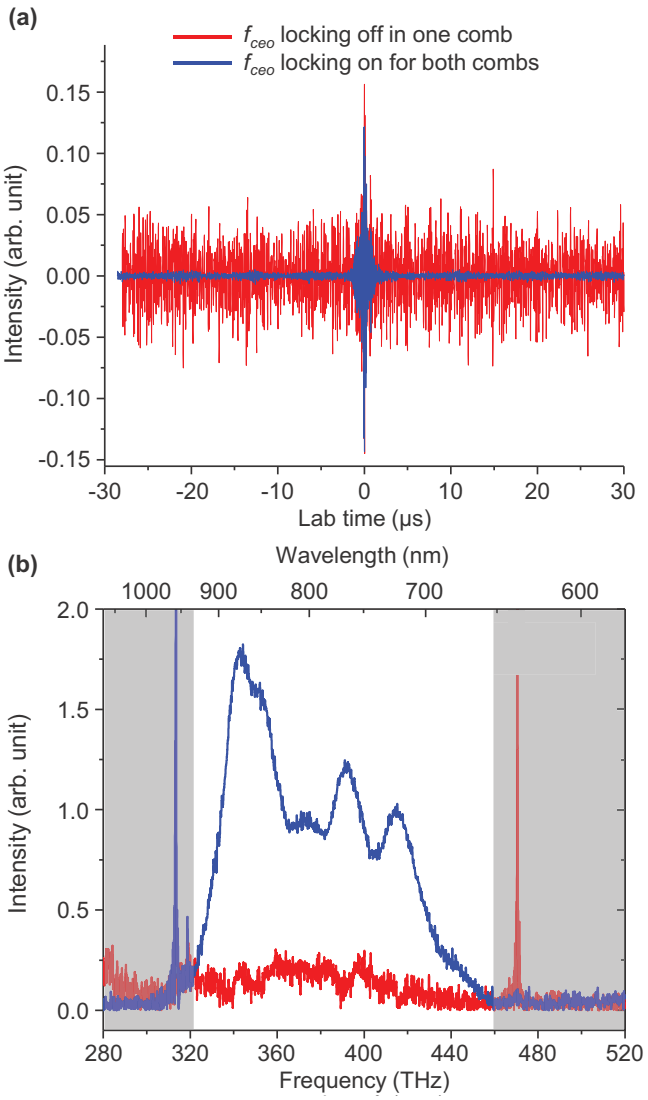

FIG. 7. Interferograms with and without f_{ceo} locking. (a) Interferogram without f_{ceo} locking in one of the combs (red) compared with both combs with f_{ceo} locking (blue). (b) Fourier transforms of interferograms in (a) where both combs had f_{ceo} locked (blue) and one of the combs had no f_{ceo} lock (red).

Before we close this subsection, a brief discussion about SNR analysis is presented. In the present work, we obtained 17 time-domain interferograms in a single scan. The single-interferogram data used to obtain the corresponding Fourier-transformed spectrum span about 6 μs, which corresponds to

167 kHz. Therefore, any acoustic noise whose frequency is lower than 167 kHz would not contribute to the noise of our signal measurement. This is one of the main reasons why we did not have to implement active stabilization schemes in our interferometric measurements. Another important noise source is a timing jitter. In our phase-locking scheme, the uncertainty δf_r in repetition frequency is about 100 μHz and that in f_{ceo} denoted as δf_{ceo} is about 10 mHz, respectively, at the integration time of 1 s. Because the repetition frequency f_r is 80 MHz, using these parameters, we can estimate the timing jitter to be 73 fs during the measurement time of 1 s. However, when we took a set of single-interferogram data for each absorption spectrum, the time span (in laboratory time) was about 6 μs. Consequently, during the data acquisition time of about 6 μs, the timing jitter would be sub-100 as, which is negligibly small compared to the optical period. This indicates that the timing jitter is not a serious source of noise. Nonetheless, it will necessary to use an active stabilization scheme for further development of the nonlinear optical DCS techniques.

E. Fourier-transformed absorption spectrum

The Fourier transforms of IR140 in ethanol (red), ethanol blank (blue), and through-air (thick gray) interferograms are shown in Fig. 8(a). The *single*-interferogram Fourier transforms are indicated by the dotted lines and compared with those with 17 averages (solid lines). The Fourier transformation for the through-air interferogram is overlaid with that measured with a spectrometer (filled gray) and this should ideally recover the laser pulse spectrum. Although there are slight differences in relative intensities of the two peaks on the blue side of the spectrum (when normalized to the maxima), the overall features show a reasonable match. Because the transmittance and absorbance spectra will be referenced to a blank background, such differences common to both the sample and reference do not affect the recovery of the molecular spectrum. In Fig. 8(a), the changes due to the sample are evident in the spectra for IR140 and ethanol blank.

Figure 8(b) shows the transmittance (red) and absorbance (blue) spectra of IR140 in ethanol recovered from a single pair of dual-comb interferograms (dotted lines) and averages of 17 spectra recovered from the interferograms (solid lines). These are compared with those measured by a spectrometer (dashed lines). The absorption band that arises from the lowest-energy dipole-allowed electronic transition of IR140 dissolved in ethanol is broad without fine features, as is typical for organic molecules in liquid phase [24]. This band spans almost 170 nm centered around 800 nm (~88 THz). With a single interferogram for the sample, the transmittance and absorbance spectra are reproduced with a signal-to-noise ratio of ~10:1. Averaging improves the signal-to-noise ratio and with only 17 averages, the recovered molecular spectrum matches that measured by a spectrometer within 2% error, for a total acquisition time of ~3.4 s for each set (one for the sample and the other of the reference).

Here, it is believed that 3.2 THz frequency resolution obtainable from a 5-μs single interferogram in the time domain would be sufficient for measuring the absorption spectrum of which linewidth is nearly 100 THz. In fact, a single-interferogram measurement capability of the present DCS technique could be useful and important in a variety of research fields. Typical chemical, biological, and nanometer-size material systems, such as fluorescent molecules; light-harvesting pigments, e.g., chlorophyll, green fluorescent protein, quantum dots; and metallic nanoparticles that absorb light in the visible frequency region, exhibit such a broad and featureless absorption spectrum. Using either ultrafast actinic pulses or high-speed solution-mixing devices, one can put the

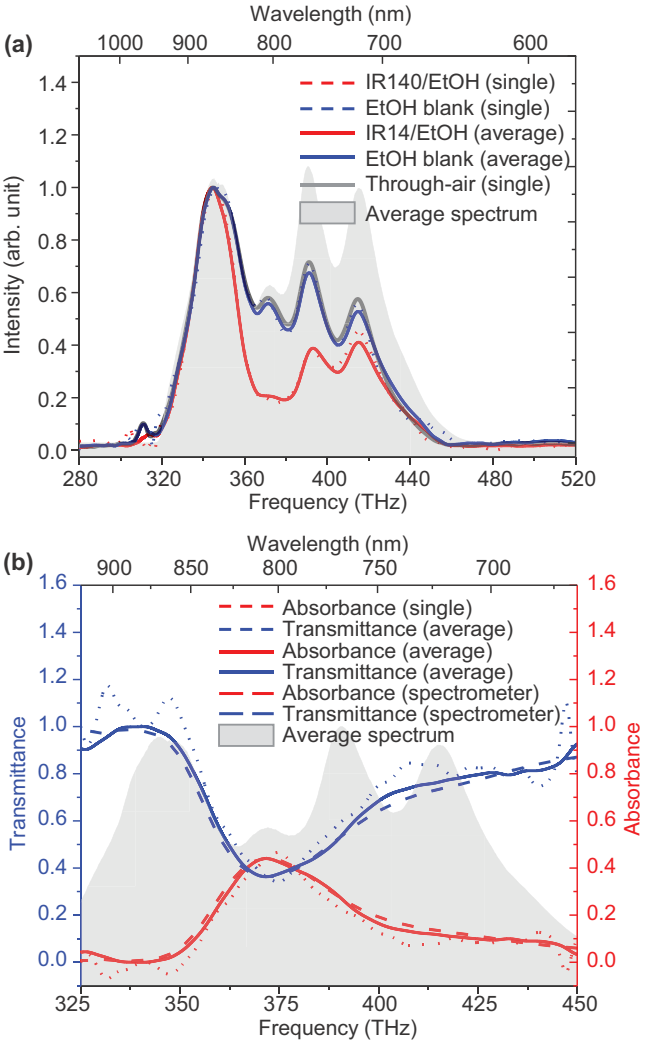

FIG. 8. Fourier-transformed spectra. (a) The spectra for the laser pulse through air (thick gray line), the ethanol blank (blue), and IR140 in ethanol sample (red) are overlaid with a laser pulse spectrum measured by a spectrometer (filled light gray). Spectra recovered from single interferograms (dotted lines) are compared with those with average of 17 spectra (solid lines) for IR140 in ethanol (red) and ethanol blank (blue). A 64-μs segment centered at the center burst containing 5121 points was Fourier transformed to obtain the spectra. The interferogram was multiplied by a 5-μs "window function" centered at the peak and zero-padded out to 3.28 ms. (b) Transmittance (blue) and absorbance (red) spectra of IR140 in ethanol recovered from a single pair of interferograms (dotted lines) are overlaid with averaged spectra from 17 pairs of interferograms (thick lines). Spectra measured with a spectrometer (dashed lines) and laser pulse spectrum (filled gray) are overlaid.

molecular system of interest on a nonequilibrium state. Then, a subsequent relaxation of the reactive molecular systems can be monitored by employing the present single-interferogram DCS without any mechanical delay stage. This can be viewed as a high-speed time-resolved interferometric detection of the time-evolved molecular spectra that directly reflect either molecular conformation or chemical structure of the reactive system under investigation.

IV. SUMMARY AND A FEW CONCLUDING REMARKS

In conclusion, a phase-locking scheme by referencing to a GPS-disciplined Rb atomic clock to synchronize combs and stabilize both f_r and f_{ceo} enabled absolute dual-comb spectroscopy to probe a quite broad molecular electronic absorption spectrum of a dye molecule in the condensed phase in the vis-NIR frequency region. Despite such large laser bandwidth and absorption width involved, few-cycle pulses containing millions of comb modes maintained stable phase coherence to allow extraction of the molecular spectrum with a single interferogram. Due to the large absorbance of the sample considered here, we did not have to use many thousands of coherent averaging [14], cavity to boost the signal [13], sophisticated phase-locking schemes [25], and/or adaptive sampling [15]. The present work should be of use in developing condensed-phase nonlinear optical measurements [26] such as transient absorption [27], second-harmonic or sum-frequency generation, and even coherent multidimensional spectroscopy [28] that critically require phase coherent detection but use only a single point detector without dispersive elements. Currently, we use the same DCS experimental setup in combination with an optical triggering system to measure a dual frequency comb transient absorption signal from a dye solution, without using any mechanical stage for controlling pump-probe delay time. We anticipate that the scanless dual-comb spectroscopy would be a useful method to study nonequilibrium molecular dynamics and chemical kinetics studies with much increased speed and sensitivity.

ACKNOWLEDGMENT

This work was supported by the Institute for Basic Science (IBS) in the Republic of Korea with Grant No. IBS-R023-D1.

[1] J. L. Hall, Rev. Mod. Phys. **78**, 1279 (2006).
[2] T. W. Hänsch, Rev. Mod. Phys. **78**, 1297 (2006).
[3] D. J. Jones, S. A. Diddams, J. K. Ranka, A. Stentz, R. S. Windeler, J. L. Hall, and S. T. Cundiff, Science **288**, 635 (2000).
[4] S. A. Diddams, D. J. Jones, J. Ye, S. T. Cundiff, J. L. Hall, J. K. Ranka, R. S. Windeler, R. Holzwarth, T. Udem, and T. W. Hänsch, Phys. Rev. Lett. **84**, 5102 (2000).
[5] S. T. Cundiff, J. Ye, and J. L. Hall, Rev. Sci. Instrum. **72**, 3749 (2001).
[6] S. T. Cundiff and J. Ye, J. Mod. Opt. **52**, 201 (2005).
[7] M. J. Thorpe, K. D. Moll, R. J. Jones, B. Safdi, and J. Ye, Science **311**, 1595 (2006).
[8] P. Fendel, S. D. Bergeson, T. Udem, and T. W. Hänsch, Opt. Lett. **32**, 701 (2007).
[9] S. A. Diddams, L. Hollberg, and V. Mbele, Nature **445**, 627 (2007).
[10] F. Adler, M. J. Thorpe, K. C. Cossel, and J. Ye, Annu. Rev. Anal. Chem. **3**, 175 (2010).
[11] I. Coddington, N. R. Newbury, and W. Swann, Optica **3**, 414 (2016).
[12] T. Ideguchi, S. Holzner, B. Bernhardt, G. Guelachvili, N. Picqué, and T. W. Hänsch, Nature **502**, 355 (2013).
[13] B. Bernhardt, A. Ozawa, P. Jacquet, M. Jacquey, Y. Kobayashi, Th. Udem, R. Holzwarth, G. Guelachvili, T. W. Hänsch, and N. Picqué, Nat. Photon. **4**, 55 (2010).
[14] I. Coddington, W. C. Swann, and N. R. Newbury, Phys. Rev. A **82**, 043817 (2010).
[15] T. Ideguchi, A. Poisson, G. Guelachvili, N. Picqué, and T. W. Hänsch, Nat. Commun. **5**, 3375 (2014).
[16] B. Lomsadze and S. T. Cundiff, Science **357**, 1389 (2017).
[17] T. Ideguchi, A. Poisson, G. Guelachvili, T. W. Hänsch, and N. Picqué, Opt. Lett. **37**, 4847 (2012).
[18] G. R. Fleming, *Chemical Applications of Ultrafast Spectroscopy* (Oxford University Press, New York, 1986).
[19] T. Ideguchi, T. Nakamura, Y. Kobayashi, and K. Goda, Optica **3**, 748 (2016).
[20] J. A. Levine, Metrologia **45**, S162 (2008).
[21] S. Koke, C. Grebing, H. Frei, A. Anderson, A. Assion, and G. Steinmeyer, Nat. Photon. **4**, 462 (2010).
[22] P. R. Griffiths and J. A. de Haseth, *Fourier Transform Infrared Spectroscopy* (Wiley, Hoboken, NJ, 2007).
[23] A. A. Ferro, J. D. Hybl, and D. M. Jonas, J. Chem. Phys. **114**, 4649 (2001).
[24] J. B. Birks, *Photophysics of Aromatic Molecules* (Wiley-Interscience, London, 1970).
[25] I. Coddington, W. C. Swann, and N. R. Newbury, Phys. Rev. Lett. **100**, 013902 (2008).
[26] S. Mukamel, *Principles of Nonlinear Optical Spectroscopy* (Oxford University Press, New York, 1995).
[27] A. Asahara and K. Minoshima, APL Photon. **2**, 041301 (2017).
[28] M. Cho, Chem. Rev. **108**, 1331 (2008).